

GLOBAL CURRENT CIRCUIT STRUCTURE IN A RESISTIVE PULSAR MAGNETOSPHERE MODEL

YUGO.E.KATO¹

¹ 2-4-21 Takewara, Matsuyama, Ehime, 790-0053, Japan

Submitted to The Astrophysical Journal

ABSTRACT

Pulsar magnetospheres have strong magnetic fields and large amounts of plasma. The structures of these magnetospheres are studied using force-free electrodynamics. To understand pulsar magnetospheres, discussions must include their outer region. However, force-free electrodynamics is limited in it does not handle dissipation. Therefore, a resistive pulsar magnetic field model is needed. To break the ideal magnetohydrodynamic (MHD) condition $E \cdot B = 0$, Ohm's law is used. In this work, I introduce resistivity depending upon the distance from the star and obtain a self-consistent steady state by time integration. Poloidal current circuits form in the magnetosphere while the toroidal magnetic-field region expands beyond the light cylinder and the Poynting flux radiation appears. High electric resistivity causes a large space scale poloidal current circuit and the magnetosphere radiates a larger Poynting flux than the linear increase outside of the light cylinder radius. The formed poloidal-current circuit has width, which grows with the electric conductivity. This result contributes to a more concrete dissipative pulsar magnetosphere model.

arXiv:1711.07471v1 [astro-ph.HE] 19 Nov 2017

1. INTRODUCTION

Electron positron pair plasma fills a pulsar's magnetosphere, which can be described using force-free electrodynamics Goldreich & Julian (1969). A time-developed method can be used to create steady pulsar-magnetosphere solutions, as suggested by Spitkovsky (2006), Komissarov (2006), McKinney (2006). Electric current flows along open magnetic-field lines whereas Poynting flux is radiated outward beyond the light cylinder.

Force-free electrodynamics has drawbacks when the electric and magnetic fields have parallel components, causing charged particles to accelerate parallel to the magnetic field line. Therefore, highly accelerated particles emit curvature radiation and pair creation occurs. This process changes the pulsar's magnetospheric structure. Deformation of the magnetosphere causes electromagnetic radiation to differ from the ideal magnetohydrodynamic (MHD) case. Therefore, the calculation of Poynting flux using force-free electrodynamics does not use the real condition.

To address this problem, resistive electromagnetic simulation has been studied. This method results in a clear global electromagnetic field structure, by which an amount of Poynting flux between the vacuum and force-free cases is radiated. Electrical conductivity dependence of global current circuit structure is revealed.

In this paper, I show that such a model can produce a steady magnetosphere. I introduce the dependence of current density on distance from the star surface. At the outer boundary, the electrical conductivity gradually decreases, making it easy to understand a pulsar magnetosphere, including its structures and its radiation mechanism.

1.1. Other research

1.1.1. Method of solving the pulsar equation

The pulsar equation is introduced by the ideal MHD condition and the force-free approximation. A scalar function of the pulsar equation gives the structure of the magnetosphere; however, this equation has a singularity in the light cylinder. The reason is that the rotational speed is limited by the speed of light. Solving the pulsar equation in all regions has become more difficult due to the presence of the singularity. Contopoulos et al. (1999) first solved the pulsar equation on both the inner and outer sides of the light cylinder using an iterative method to connect them. Gruzinov (2005) examined the structure of the surrounding separatrix in the equatorial plane. Timokhin (2006) showed the solution for a different closed magnetosphere.

1.1.2. Time-developed method

In quasi-analytic methods, the stability of solutions is unknown; the time-developed method, however, can obtain stable solutions. Spitkovsky (2006) found a 3D inclined rotator solution; Komissarov (2006) obtained a result using a 2D axisymmetric fully relativistic MHD code, and McKinney (2006) did so using a force-free code. Tchekhovskoy et al. (2013) obtained a result using 3D oblique rotator fully relativistic MHD.

One weak point of this method is that electric-particle motion is neglected. The force-free method is limited as it cannot handle pair creation.

1.1.3. Particle-in-cell method

Maxwell's equations for the electromagnetic field and charged particles constitute equations of motion, which can be solved by time integration. The electromagnetic field is calculated at each point of the grid. The position and velocity of the particles are calculated using the equations of motion. A non-zero number of particles in a grid is required to represent a plasma magnetosphere. Indeed, a large number of particles is needed to match the above conditions in all calculation regions, but computers cannot handle such numbers due to limited memory size. Therefore, the ratio of superparticle electric charge and mass is different from that of real particles. In particle-in-cell method, a simple pair creation model is used, and it differs for each author. Furthermore, the result magnetosphere strongly depends on pair creation model.

In the case without active pair creation, the pulsar magnetosphere has two charged clouds in the polar and equatorial regions. This is known to describe a pulsar with a disc-dome configuration (Krause-Polstorff & Michel 1985). This solution is not stable and experiences diocotron instability as shown by Pétri (2009).

Philippov & Spitkovsky (2014) applied a sufficient pair plasma to obtain a nearly force-free aligned rotator solution. Cerutti et al. (2015) found the same result. Chen & Beloborodov (2014) combined pair creation and an axisymmetric magnetosphere; their simulation did not result in pair creation. Philippov et al. (2015) described a generalized-inclination rotator, whereas Cerutti et al. (2016) showed a 3D-PIC simulation.

1.1.4. Resistive Force-free Format

The resistive force-free format adds electrical resistivity to the force-free approximation. In the case where electrical conductivity limit is very high, the result is expected to approach the force-free approximation. The current density formula is derived from Ohm's law. The

time development of Maxwell equations and the current-density equation shows a steady solution.

A current density model was first applied to a pulsar magnetosphere by Lyutikov (2003). This model is derived from Ohm's law, but has one free parameter: the velocity along the magnetic field line. In order to simplify this equation, Lyutikov (2003) set the velocity along the magnetic field to zero.

The characteristic of this current density model gives a space-like electromagnetic field. Some works present different results from the ideal MHD case. Different current densities model different magnetospheric solutions. The structure of the current sheet and the emitted Poynting flux are different. Poynting Gruzinov (2007), Gruzinov (2008) noticed the sign of the current density four-vector. The space-like current-density region differs from the case of ideal MHD.

Li et al. (2011) shows the Poynting flux dependence of $(\sigma/\omega)^2$. The poynting flux of the magnetosphere has been obtained as an intermediate value in the vacuum and force-free cases.

So far, the shape and width of the electric current have not been examined. Therefore, I consider these properties under change to the global region of current flow.

2. CURRENT DENSITY MODEL

2.1. Force-free electromagnetic fields

In the case of the force-free approximation, the current density is uniquely determined by electromagnetic fields under the ideal MHD condition. The explicit form will be derived below. The force-free condition is written as

$$\rho c \mathbf{E} + \frac{\mathbf{j} \times \mathbf{B}}{c} = 0. \quad (1)$$

By the cross product to eq. (1) with \mathbf{B} and using a vector calculus identity, we have

$$\mathbf{j} = \rho c \frac{\mathbf{E} \times \mathbf{B}}{B^2} + \frac{(\mathbf{j} \cdot \mathbf{B})\mathbf{B}}{B^2}, \quad (2)$$

where $B^2 \neq 0$ has been assumed. We also assume that the ideal MHD condition $\mathbf{E} \cdot \mathbf{B} = 0$ always holds, such that the time derivative is also zero.

$$\frac{\partial}{\partial t}(\mathbf{E} \cdot \mathbf{B}) = \frac{\partial \mathbf{E}}{\partial t} \cdot \mathbf{B} + \mathbf{E} \cdot \frac{\partial \mathbf{B}}{\partial t} = 0. \quad (3)$$

The time-derivative terms of the electromagnetic fields are substituted by the Maxwell equations, and eq. (3) becomes

$$(\nabla \times \mathbf{B}) \cdot \mathbf{B} - \frac{4\pi}{c} \mathbf{j} \cdot \mathbf{B} - (\nabla \times \mathbf{E}) \cdot \mathbf{E} = 0. \quad (4)$$

By eliminating the term $\mathbf{j} \cdot \mathbf{B}$ from eq (2), the current density is given by

$$\frac{4\pi}{c} \mathbf{j} = \frac{(\nabla \cdot \mathbf{E})\mathbf{E} \times \mathbf{B}}{B^2} + \frac{\mathbf{B} \cdot (\nabla \times \mathbf{B}) - \mathbf{E} \cdot (\nabla \times \mathbf{E})}{B^2} \mathbf{B} \quad (5)$$

where the charge density ρ is replaced by Gauss's law, $\nabla \cdot \mathbf{E} = 4\pi\rho$.

The first term in eq.(5) is the $\mathbf{E} \times \mathbf{B}$ drift. If $|E| < |B|$, then there is a frame in which the electric field vanishes. The velocity of this frame measured in the lab frame is $\mathbf{E} \times \mathbf{B}/B^2$. Unfortunately, the condition $|E| < |B|$ is not guaranteed in the dynamics. Physically, if $|E| > |B|$ happens elsewhere, strong currents should flow to reduce the electric field. In the numerical calculation, this effect should be included by hand to construct proper force-free fields. The second term in eq.(5) describes the current flow along the magnetic field. In this way, the current density is determined uniquely for given \mathbf{E}, \mathbf{B} in the force-free approximation. The electromagnetic fields \mathbf{E} and \mathbf{B} should be solved with the source (5) involving the spatial derivatives of \mathbf{E} and \mathbf{B} . Thus, causal structure, i.e., information propagation with light velocity c , is broken in this approximation.

2.2. Resistive scheme

We here derive another current model described by electromagnetic fields, namely the resistive model proposed by Li et al. (2011). Our basic assumption is Ohm's law, which in the fluid rest frame is

$$\mathbf{j}_{\text{fluid}} \equiv \sigma \mathbf{E}_{\text{fluid}}, \quad (6)$$

where σ is the electric conductivity.

The relation between the current density and the electromagnetic fields in the laboratory frame is given by the Lorentz transformation. We consider a frame where the electric and magnetic fields are parallel. The fluid rest frame is given by the Lorentz boost β_1 along the parallel. The laboratory frame is given by another boost, β_{\parallel} , in the $\mathbf{E} \times \mathbf{B}$ direction. Thus, the laboratory frame can be connected to the fluid rest frame through two boosts with β_1 and β_{\parallel} . After some algebra, we have

$$\mathbf{j} = \frac{\rho_e c \mathbf{E} \times \mathbf{B}}{B^2 + E_0^2} + \frac{(-\beta_{\parallel} \rho_e c + \sqrt{\frac{B^2 + E_0^2}{B_0^2 + E_0^2}} (1 - \beta_{\parallel}^2) \sigma E_0) (B_0 \mathbf{B} + E_0 \mathbf{E})}{B^2 + E_0^2} \quad (7)$$

where E_0 and B_0 are given by two Lorentz invariants defined by ($E_0 > 0$)

$$E_0^2 - B_0^2 = \mathbf{E}^2 - \mathbf{B}^2, \quad (8)$$

$$E_0 B_0 = \mathbf{E} \cdot \mathbf{B}. \quad (9)$$

They are explicitly solved as

$$B_0^2 = \frac{1}{2} \left(\mathbf{B}^2 - \mathbf{E}^2 + \sqrt{(\mathbf{B}^2 - \mathbf{E}^2)^2 + 4(\mathbf{E} \cdot \mathbf{B})} \right), \quad (10)$$

$$E_0 = \sqrt{B_0^2 - \mathbf{B}^2 + \mathbf{E}^2}, \quad (11)$$

$$B_0 = \text{sign}(\mathbf{E} \cdot \mathbf{B}) \sqrt{B_0^2}. \quad (12)$$

The magnitude of β_{\parallel} is given by

$$\beta_{\parallel} = \sqrt{\frac{B^2 - B_0^2}{B^2 + E_0^2}}. \quad (13)$$

There remains one parameter, β_{\parallel} , which describes fluid speed in the direction of the magnetic field.

The current density from eq. (7) can also be expressed by \mathbf{E} and \mathbf{B} only, as in the force-free case. By introducing E_0 , the velocity in the first term is always less than c . The velocity is furthermore reduced to the standard drift-velocity in the case where $\mathbf{E} \cdot \mathbf{B} = 0$.

The second important point is the fact that eq. (7) is expressed by \mathbf{E} and \mathbf{B} without spatial derivatives other than the charge density. This is in contrast to the force-free case.

2.3. Speed along the magnetic field

We here discuss the parameter β_{\parallel} , which describes the fluid velocity in the direction of the magnetic-field line. This quantity should be determined only by physical argument. Gruzinov (2011) proposed that the relativistic four-current vector (ρ_e, \mathbf{j}) should be space-like. This condition determines β_{\parallel} as

$$\beta_{\parallel} = \frac{-\rho_e}{\sqrt{\gamma_x^2 \sigma^2 E_0^2 + \rho_e^2 c^2}}. \quad (14)$$

With this choice, eq. (7) becomes

$$\mathbf{j} = \frac{\rho_e c \mathbf{E} \times \mathbf{B}}{B^2 + E_0^2} + \frac{\sqrt{\gamma_x^2 \sigma^2 E_0^2 + \rho_e^2 c^2} (B_0 \mathbf{B} + E_0 \mathbf{E})}{B^2 + E_0^2}, \quad (15)$$

where γ_x is given by

$$\gamma_x^2 = \frac{B^2 + E_0^2}{B_0^2 + E_0^2}. \quad (16)$$

Space-like four current may not be adequate for the pulsar magnetosphere. Within closed magnetic field lines, charge-separated plasma co-rotates with the central star. However, this condition may not hold in the open-field-line region.

Li et al.(2012) assumed $\beta_{\parallel} = 0$; i.e., the velocity parallel to the magnetic field is slowest. This assumption may not be justified, but eq. (7) has the simple form

$$\mathbf{j} = \frac{\rho_e c \mathbf{E} \times \mathbf{B} + \sqrt{\frac{B^2 + E_0^2}{B_0^2 + E_0^2}} \sigma E_0 (B_0 \mathbf{B} + E_0 \mathbf{E})}{B^2 + E_0^2}. \quad (17)$$

In our numerical calculation, we adopt this type of current model.

2.4. Correspondence between the force-free and vacuum solutions

When electrical conductivity $\sigma = 0$ and electric charge $\rho_e = 0$ in the vacuum; the force-free approximation corresponds to $\sigma = \infty$. The toroidal field current sheet is formed on the equatorial plane in the force-free approximation, but not in the vacuum case as no current flows in the vacuum.

The amount of current flowing through the magnetosphere will vary depending on the electrical conductivity σ . Poynting flux does not diverge in the limit of infinite electrical conductivity because there are no more vacuum gaps.

2.5. Difference in the solution due to the current density model

In the case of force-free electrodynamics, the form of the electric current is unique. In the resistive force-free scheme, the expression of the current density is not determined uniquely, because the speed in the magnetic field line direction is a free parameter. Li et al. (2012) set $\beta_{\parallel} = 0$. The region where magnetic field lines are closed is formed properly in the case of the uniform electrical conductivity. Poloidal current flows in the region where the magnetic field lines are open. On the other hand, different current densities in the model proposed by Gruzinov (2007). Gruzinov proposed a current density model to satisfy the space-like current density conditions. But, it remains unclear whether this current density model is valid or not for pulsar magnetospheres.

3. NUMERICAL METHOD AND PROBLEM SETUP

3.1. Electromagnetic fields

Maxwell's equations are solved with the charge density ρ_e and the current density \mathbf{j} :

$$\frac{1}{c} \frac{\partial \mathbf{B}}{\partial t} = -\nabla \times \mathbf{E}, \quad (18)$$

$$\frac{1}{c} \frac{\partial \mathbf{E}}{\partial t} = \nabla \times \mathbf{B} - \frac{4\pi \mathbf{j}}{c}, \quad (19)$$

$$\nabla \cdot \mathbf{B} = 0, \quad (20)$$

$$\nabla \cdot \mathbf{E} = 4\pi \rho_e. \quad (21)$$

In order to solve these equations, we use a scalar potential Φ and a vector potential \mathbf{A} satisfying the Coulomb gauge, $\nabla \cdot \mathbf{A} = 0$. For axially symmetric fields, the

following form given by two functions, $F(t, r, \theta)$ and $G(t, r, \theta)$, is automatically satisfied with the gauge condition:

$$\mathbf{A} = \frac{1}{r \sin \theta} \nabla F \times \mathbf{e}_\phi + \left(\frac{G}{r \sin \theta} \right) \mathbf{e}_\phi, \quad (22)$$

where \mathbf{e}_ϕ is a unit vector in the azimuthal direction. The magnetic field \mathbf{B} is given by $\nabla \times \mathbf{A}$:

$$\mathbf{B} = \frac{1}{r \sin \theta} \nabla G \times \mathbf{e}_\phi + \left(\frac{S}{r \sin \theta} \right) \mathbf{e}_\phi, \quad (23)$$

where the function S in B_ϕ is given by

$$S = -\mathcal{D}F, \quad (24)$$

and the differential operator \mathcal{D} is defined by

$$\mathcal{D} \equiv \frac{\partial^2}{\partial r^2} + \frac{\sin \theta}{r^2} \frac{\partial}{\partial \theta} \left(\frac{1}{\sin \theta} \frac{\partial}{\partial \theta} \right). \quad (25)$$

The electric field \mathbf{E} is expressed by the time derivative of \mathbf{A} and the gradient of Φ :

$$\mathbf{E} = -\nabla \Phi - \frac{\partial}{c \partial t} \mathbf{A} \quad (26)$$

$$= -\nabla \Phi - \frac{1}{r \sin \theta} \nabla \left(\frac{\partial F}{c \partial t} \right) \times \mathbf{e}_\phi - \left(\frac{1}{r \sin \theta} \frac{\partial G}{c \partial t} \right) \mathbf{e}_\phi. \quad (27)$$

The electric field (eq.(27)) is given by the time derivative of F such that it is convenient to solve the time derivative of eq.(24), i.e.,

$$\mathcal{D} \left(\frac{\partial F}{\partial t} \right) = -\frac{\partial S}{\partial t}. \quad (28)$$

Substituting these forms (eqs.(23) and (27)) into eq.(19), we have two wave equations for G and S . They are the ϕ component and the rotation of the poloidal component of eq.(19):

$$\left(\frac{1}{c^2} \frac{\partial^2}{\partial t^2} - \mathcal{D} \right) G = \frac{4\pi}{c} j_\phi r \sin \theta, \quad (29)$$

$$\left(\frac{1}{c^2} \frac{\partial^2}{\partial t^2} - \mathcal{D} \right) S = \frac{4\pi}{c} \left(\frac{\partial(rj_\theta)}{\partial r} - \frac{\partial j_r}{\partial \theta} \right) \sin \theta. \quad (30)$$

From eq.(21), we have the Poisson equation for Φ :

$$\left(\frac{1}{r^2} \frac{\partial}{\partial r} \left(r^2 \frac{\partial}{\partial r} \right) + \frac{1}{r^2 \sin \theta} \frac{\partial}{\partial \theta} \left(\sin \theta \frac{\partial}{\partial \theta} \right) \right) \Phi = -4\pi \rho_e. \quad (31)$$

One advantage to the potential formalism is that the constraints, eqs.(18) and (20), are automatically satisfied.

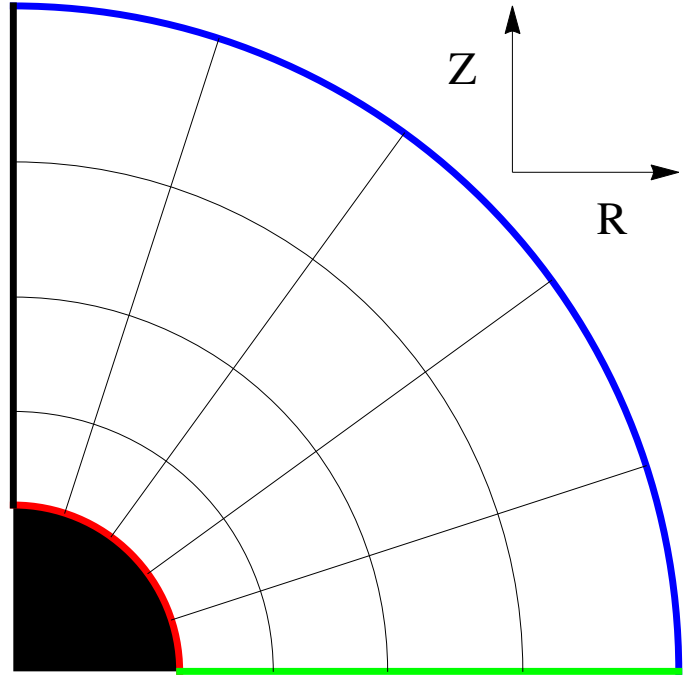


Figure 1. Figure of the two dimensional computational domain and four boundaries. The thin black line represents the grid. The red line is star surface, thick black line is the rotation and magnetic axis, the green line is the equatorial plane, and the blue line represents the outer boundary.

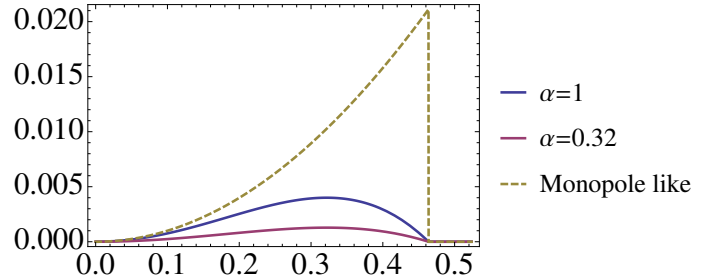


Figure 2. The structure of the surface toroidal flux function $S_0(r = r_0, \theta)$

3.2. Region

In our numerical calculation, we use the spherical coordinate (r, θ) with range $r_0 \leq r \leq r_{\text{out}}$, and $0 \leq \theta \leq \pi/2$. Typically, we set $r_{\text{out}}/r_0 = 60$. The light cylinder, R_L , is located at $R_L/r_0 = 1/\Omega = 5$. We use the finite difference method to solve the partial differential equations. The typical numbers of cells on the grid are 60 and 96 in the r and θ directions, respectively. The grid-cell spacing in the radial direction is taken as $\Delta r \propto r^{1/2}$ to obtain fine resolution near the inner region, whereas the spacing in the angular direction is constant.

3.3. Boundary conditions

In this section, we discuss the boundary conditions. First, we consider the condition at the inner boundary r_0 . The poloidal magnetic field there is a dipole field given by

$$\mathbf{B}_d = [B_r, B_\theta, B_\phi] = \left[\frac{2\mu \cos \theta}{r^3}, \frac{\mu \sin \theta}{r^3}, 0 \right], \quad (32)$$

where μ is the dipole moment and the field strength on the pole r_0 is $B_0 = 2\mu/r_0^3$. The magnetic flux function G for a purely dipole field is given by

$$G_d = \frac{\mu \sin^2 \theta}{r}. \quad (33)$$

We always fix the function G at $r = r_0$ as

$$G(r_0, \theta) = \frac{\mu \sin^2 \theta}{r_0}. \quad (34)$$

Thus, the continuity of the radial component B_r is guaranteed.

Inside the surface $r \leq r_0$, the ideal MHD condition holds such that the electric field is given by the rotational velocity $\mathbf{v} = (r \sin \theta)\Omega \mathbf{e}_\phi$ and the magnetic-dipole field

$$\mathbf{E} = -\mathbf{v} \times \mathbf{B}_d = \left[\frac{\mu \Omega \sin^2 \theta}{r_0^2}, -\frac{2\mu \Omega \cos \theta \sin \theta}{r_0^2}, 0 \right]. \quad (35)$$

The θ component is given by $E_\theta = -\Omega \partial G_d / \partial \theta$. From the continuity of E_θ , the electric potential Φ at the surface can be chosen as

$$\Phi(r_0, \theta) = \frac{\mu \Omega \sin^2 \theta}{r_0}, \quad (36)$$

and

$$\frac{\partial F}{\partial t} = 0. \quad (37)$$

Next, we consider the toroidal magnetic field, $B_\phi = S/(r \sin \theta)$. For the force-free case, the current function S is given by a function of G . In particular, in the split-monopole solution, the toroidal magnetic flux is given by

$$S_m = -\Omega G_m \left(2 - \frac{G_m}{B_0 r_0^2} \right), \quad (38)$$

and $G_m = B_0 r_0^2 (1 - \cos \theta)$, where B_0 is a constant, $B_r = B_0 (r_0/r)^2$. The toroidal magnetic flux can also be expressed as a function of θ by eliminating G_m :

$$S_m = -\Omega B_0 r_0^2 \sin^2 \theta. \quad (39)$$

The current function should vanish for the rotating dipole in the region $\theta > \theta_p$ at the surface, where θ_p is the polar-cap angle $\sin \theta_p = (\Omega r_0)^{1/2}$. We expect that the magnetic field near the pole, even for a rotating dipole,

will be similar to that in the split-monopole case. At the same time, the functional form (39) should be truncated for $\theta > \theta_p$. Our choice of S at r_0 is a simple quadratic function of $\sin^2 \theta$:

$$S(r_0, \theta) = -\frac{2\mu \Omega}{r_0} \sin^2 \theta \left[1 - \frac{\sin^2 \theta}{\sin^2 \theta_p} \right], \quad (40)$$

where the coefficient B_0 is replaced by the dipole moment $B_0 = 2\mu/r_0^3$.

In Fig. 2, we compare the functions eq.(40) and eq.(39) truncated at θ_p . The sharp drop of eq.(39) at θ_p means that there is a current sheet there. Our choice, (40), smoothly goes to zero at θ_p , but the strength is much smaller. In order to examine this fact, we use in the numerical calculation αS multiplied by a factor α .

Here we summarize the values at the inner boundary r_0 :

$$E_\theta = -\frac{2\mu \Omega \cos \theta \sin \theta}{r_0^2}, \quad (41)$$

$$E_\phi = 0, \quad (42)$$

$$B_r = -\frac{2\mu \cos \theta}{r_0^3}, \quad (43)$$

$$B_\phi = \begin{cases} -\frac{2\alpha \mu \Omega}{r_0^3} \sin \theta \left[1 - \frac{\sin^2 \theta}{\sin^2 \theta_p} \right] & (\theta \leq \theta_p) \\ 0 & (\theta > \theta_p). \end{cases} \quad (44)$$

On the other hand, the remaining components, E_r and B_θ , cannot be specified. They are given by radial derivative of the potentials.

The other boundary conditions are almost clear. On the pole $\theta = 0$, E_θ, E_ϕ and B_θ, B_ϕ should vanish, such that the functions should satisfy the condition on the pole

$$G(r, 0) = 0, \quad S(r, 0) = 0, \quad F(r, 0) = 0, \quad \frac{\partial \Phi(r, 0)}{\partial \theta} = 0. \quad (45)$$

We assume a symmetry with respect to the equator such that $E_\theta = 0, B_\phi = 0$. On the equator, the boundary conditions for S, F and Φ are

$$S(r, \pi/2) = 0, \quad F(r, \pi/2) = 0, \quad \frac{\partial \Phi(r, \pi/2)}{\partial \theta} = 0. \quad (46)$$

The conditions for the magnetic flux function G are different inside and outside the light cylinder Ω^{-1} . The magnetic flux function G for $r < \Omega^{-1}$ is

$$\frac{\partial G(r, \pi/2)}{\partial \theta} = 0 \quad (47)$$

whereas that for $r \geq \Omega^{-1}$

$$G(r, \pi/2) = G_0, \quad (48)$$

where G_0 is a constant describing the last open field line.

Finally, at the outer boundary, we impose outgoing condition. In order to remove numerical reflection at the outer boundary, the size r_{out} is set to a sufficiently large value, and the simulation time is limited to $t \leq r_{out}$.

3.4. Electrical conductivity σ

The current model eq. (17) has electrical conductivity σ . Electrical conductivity σ depends on r by the following formula:

$$\sigma(r) = \frac{\sigma_0}{r^n}. \quad (49)$$

Here, σ_0 is the electrical conductivity of the surface $\sigma_0 = \sigma(r = 1)$; n is r -dependence parameter. The electrical conductivity is large in the vicinity of the star and falls off with increasing radial distance. The outer boundary is set to an almost-vacuum condition. We now consider each of the electrical-conductivity parameters $\sigma_0 = 2, 5, 10, 20, 50, 100$ in the $n = 2$ case.

4. RESULT

4.1. The structure of the obtained solution

The dynamical equations (29), (30), (31), and (17) are integrated by time, and almost stationary solutions are obtained after several wave-crossing periods. Steady states appeared under each electrical conductivity parameter $\sigma_0 = 2, 5, 10, 20, 50, 100$ in the $n = 2$ case. The results for $n = 2$ and $\sigma_0 = 10, 50$ are explained in the next section.

4.1.1. Poloidal magnetic field, G

The dynamical equations are integrated by time, and almost-stationary solutions are obtained after several wave-crossing periods. From the star surface to the outside area, the magnetosphere gradually becomes a steady state. Specifically, the magnetic field at radius $r = 30$ became steady over the time period $t = 50$. I explain the formation of the magnetic field in terms of its poloidal and toroidal components separately. Figure 3(a) shows the steady state magnetic fields $n = 2, \sigma_0 = 10$ in the meridian plane. The red line in Fig. 3(a) is a light cylinder of radius $R = R_{LC} = 5$. The black solid lines represent the flux functions $G/(\mu/r_0) = 0.05, 0.1, \dots, 0.4$, normalized by the dipole poloidal magnetic flux in surface. In particular, the thick black line of Fig 3(b) is $G/(\mu/r_0) = 0.2$. The magnetic field lines, $G = 0.2$, pass through the light cylinder in the case of the magnetic dipoles. For comparison, those for the magnetic dipole are also shown by black dashed lines with the same values, $G_d/(\mu/r_0) = 0.05, 0.1, \dots, 0.4$. The lines with $G/(\mu/r_0) < 0.285$ are open outwardly,

and the others are closed within the light cylinder. Both lines for the dipolar and numerical results of, e.g., $G/(\mu/r_0) = 0.05$, are parallel for $r/r_0 < 3$, but they are significantly separated beyond the light cylinder. The line for the vacuum dipole is closed, whereas that for our numerical result is open, and the structure becomes almost radial. Open and closed magnetic-field lines feature the same force-free-electrodynamics pulsar solution. The magnetic field is very strong and it moves with the plasma; it cannot co-rotate because the co-rotation speed outside of the light cylinder exceeds the speed of light. Thus, the magnetic-field lines are open for the outside. Specifically, $G = 0.285$ in the equatorial plane is greater than 0.2, toroidal current form a poloidal magnetic fields in the vicinity last open field line. Next, I show the result of changing the electrical-conductivity parameter σ_0 . Fig. 3(a) and Fig.3(c) respectively correspond to the electrical conductivities $\sigma_0 = 10$ and 50. Comparison of these two figures show that they exhibit poloidal magnetic fields of the same shape.

4.1.2. Toroidal magnetic field S

The toroidal magnetic field $B_\phi = S/R$ is also shown in Fig. 3(a). The color contour represents $S/(\mu/r_0^2)$. Red and blue indicate negative and positive values, respectively. The maximum value of S is located inside the light cylinder.

Fig. 3(b) shows the magnetic field near the star surface. According to Figure 3(b), the toroidal field S has a negative value in the $G < 0.2$ region and a positive value in the $G > 0.2$ area near the equatorial plane. The poloidal current inwardly flows in the polar region, i.e., the region from the z -axis to the maximum with respect to θ , whereas the current outwardly flows along the last open line in the equatorial region. The toroidal magnetic field S gradually goes to zero outwardly due to resistivity and spreads to the outside beyond the light cylinder. No toroidal magnetic field, S , exists near the pole. This result is due to spatial symmetry.

Fig. 4 shows the time averaged toroidal flux S in $\theta = 0.74$. The toroidal magnetic field S decreases gradually by the radius from the star. The maximum value of S falls inside the light cylinder radius. The maximum value does not match the radius of the light cylinder. The concentrated poloidal current area is the light cylinder interior.

The toroidal magnetic field, S , increases due to large electrical conductivity σ_0 . In our model, the value increases with the increase of r eq. (49). The toroidal magnetic field increase proportionally to electrical conductivity. Fig.3(c) shows the electromagnetic field for $\sigma_0 = 50$, five times bigger than the $\sigma_0 = 10$ case. In

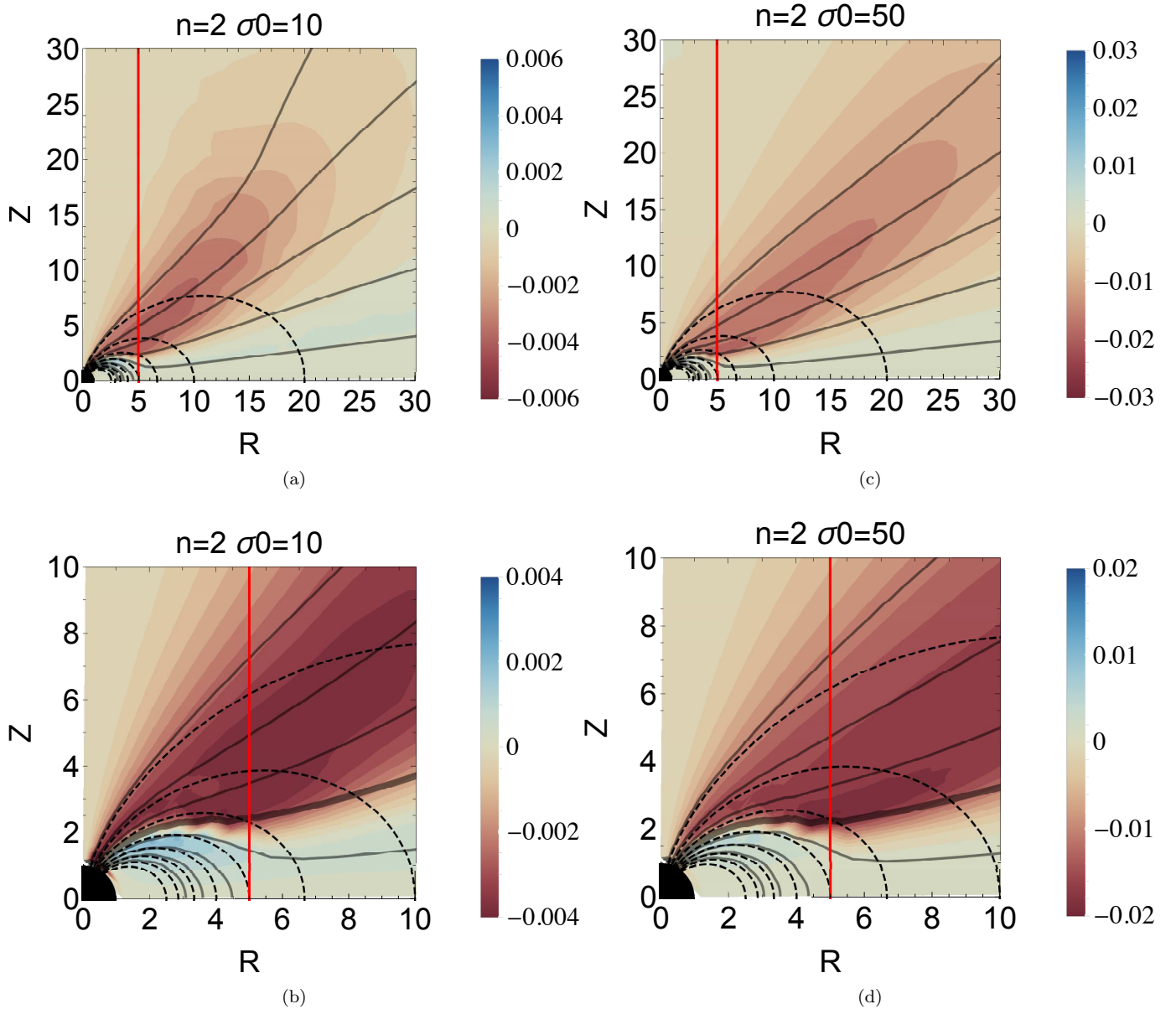


Figure 3. Poloidal and toroidal magnetic fields in the meridian plane for $\sigma_0 = 10, 50$. The light cylinder radius $R_{LC} = c/\Omega$ is shown by a red vertical line. The poloidal magnetic field line is solid and black. The dashed black lines show the magnetic dipole poloidal magnetic fields. The toroidal magnetic strength is indicated by contour color. Bottom is zoom in view.

addition, this field area spreads out. This is in contrast to the poloidal magnetic field G , which is not changed by the electrical conductivity.

4.1.3. Electrostatic potential Φ

Fig. 5(a) shows the electrostatic potential contour of $\sigma_0 = 10$. From $\Phi = 0.01$ to 0.08, contours are equally spaced for each 0.01. In the numerical calculation, the electrostatic potential on the star's surface does not change with time because of the boundary conditions eq. (36). Blue lines in Fig. 5(a) spread out from the surface boundary and extend in the radial direction.

Blue lines are connected vertically towards the equatorial plane because the field's boundary condition has only an R component in this plane. Fig. 5(b) shows the electrostatic potential of the spatial region from $Z = 0$ to 30. Here, we have drawn the contour line in increments of 0.005 from $\Phi = 0.04$.

The densities of the equipotential lines are proportional to the strength of the electric field, which is strong on the star surface and decreases as one goes radially outward. No electric field dominant ($E^2 - B^2 > 0$) area exist in $1 \leq r \leq 30$. The magnetic field in the obtained results is always stronger than the electric field.

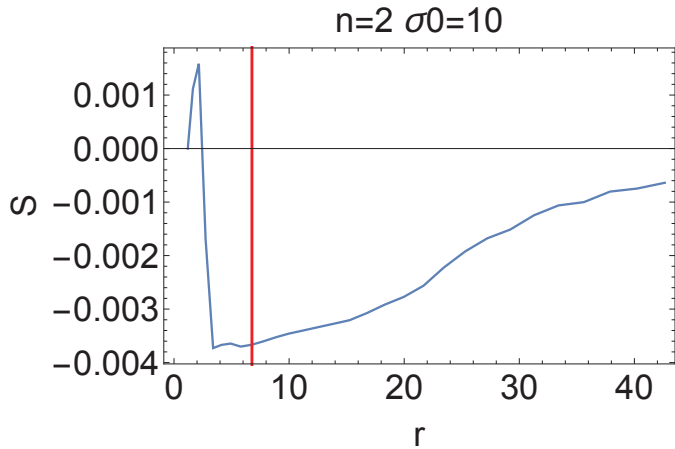


Figure 4. Time-averaged toroidal magnetic flux function S for the center of the star. $\theta = 0.74$

Fig.5(c) is the drawn contours of the $\sigma_0 = 50$ electrostatic potential cases. Electrical conductivity σ_0 increases along with the electrostatic potential of the equatorial plane. However, the difference of electrostatic potential of the equatorial plane between the $\sigma_0 = 10$ and $\sigma_0 = 50$ is about 10%.

When the electrical conductivity is different from this case, the overall structure of the solution remains similar. For example, electrical conductivity is increased in a toroidal magnetic field, but little shape change was observed about the potential.

4.1.4. Poloidal current j_p

Current density is divided into poloidal and toroidal components. The poloidal component of current density j_p consists of j_r and j_θ .

$$j_p = \sqrt{j_r^2 + j_\theta^2}. \quad (50)$$

Fig. 6(a) plots the magnitude of the poloidal current density at electric conductivity $\sigma_0 = 10$. The yellow region has a large current density; the blue region has a small current density. Fig. 6(a) shows that an electric circuit forms in the magnetosphere. Fig. 6(d) shows the poloidal current density $j_p r^2$ for $\sigma_0 = 50$. Both figures exhibit the same poloidal current circuit structure. I divide three parts to understand the mechanics of the poloidal current density distribution. Fig. 9 shows a current circuit schematic diagram. The oblique lines in the central region indicate low poloidal current density. The arrows A and B are the current inside of the light cylinder; both parts of current flow along the magnetic field line but in opposite directions. Arrow C indicates current that does not flow along the magnetic field, but

returns inside. The total current flow composes the current circuit and gives rise to the toroidal magnetic field. Poloidal current makes the toroidal magnetic field. The oblique lines in the region near the star indicate a dead zone. In this region, plasma co-rotates with the star; thus, the poloidal current does not exist.

The r-component electric field E_r is formed on the star surface. Therefore, current flows to the inside of θ_{pc} from the star surface. The poloidal current density, j_r , at $\theta_{neutral}$ is zero. The $\theta_{neutral}$ star surface represents a boundary at which the direction of the poloidal current is interchanged. Where $0 < \theta < \theta_{neutral}$ (Arrow A), $j_r < 0$ because there is a current toward the star. In addition, there is a current flowing outward from the star, $\theta_{neutral} < \theta < \theta_p$ (Arrow B). The region $\theta > \theta_p$ is a closed zone in which poloidal current does not flow, meaning that there is a region of low poloidal density besides the star's surface. The concentration of poloidal current caused by the Lorentz force. Concentration of the current occurs on the upper and lower sides (Arrow A and Arrow B). The poloidal current density of the open magnetic field lines for the area outside of the light cylinder also spread spatially. Focusing on large areas of lower current density (Arrow C), and has a distribution that across the magnetic field lines. This corresponds to a large Z component of the current vector. In order to clarify, I compare the magnitudes of poloidal current in different component sections.

Figs. 6(b) and (c) are obtained by drawing a distribution of the first term and the absolute value of the second term of the poloidal current equation (17). The $B_\phi E_r$ component of the first term becomes dominant due to the fact that the electrical conductivity σ decreases outward, making the second term small. The current along the magnetic field hardly flows to the outside because it is assumed that the electrical conductivity σ has a spatial dependence. Also, the electric field has a component perpendicular to the magnetic field. The poloidal current perpendicular to the magnetic field is generated by the electric field. Therefore, the flow of current toward the star across the magnetic-field lines occurs gradually. When this flow returns to the star, one round of the current circuit is formed. Figs. 7 and 8 are obtained by drawing the direction of the vector of the poloidal currents. The strength of the poloidal current is increased toward the red from the blue.

Fig. 6(d) illustrates the poloidal current density at electric conductivity $\sigma_0 = 50$. In the case of $\sigma_0 = 20$, the $j_p = 0$ area is eliminated by $r = 10$. In the case of $\sigma_0 = 50$, the poloidal current density distribution is changed, as shown in 6(d); this is because the compo-

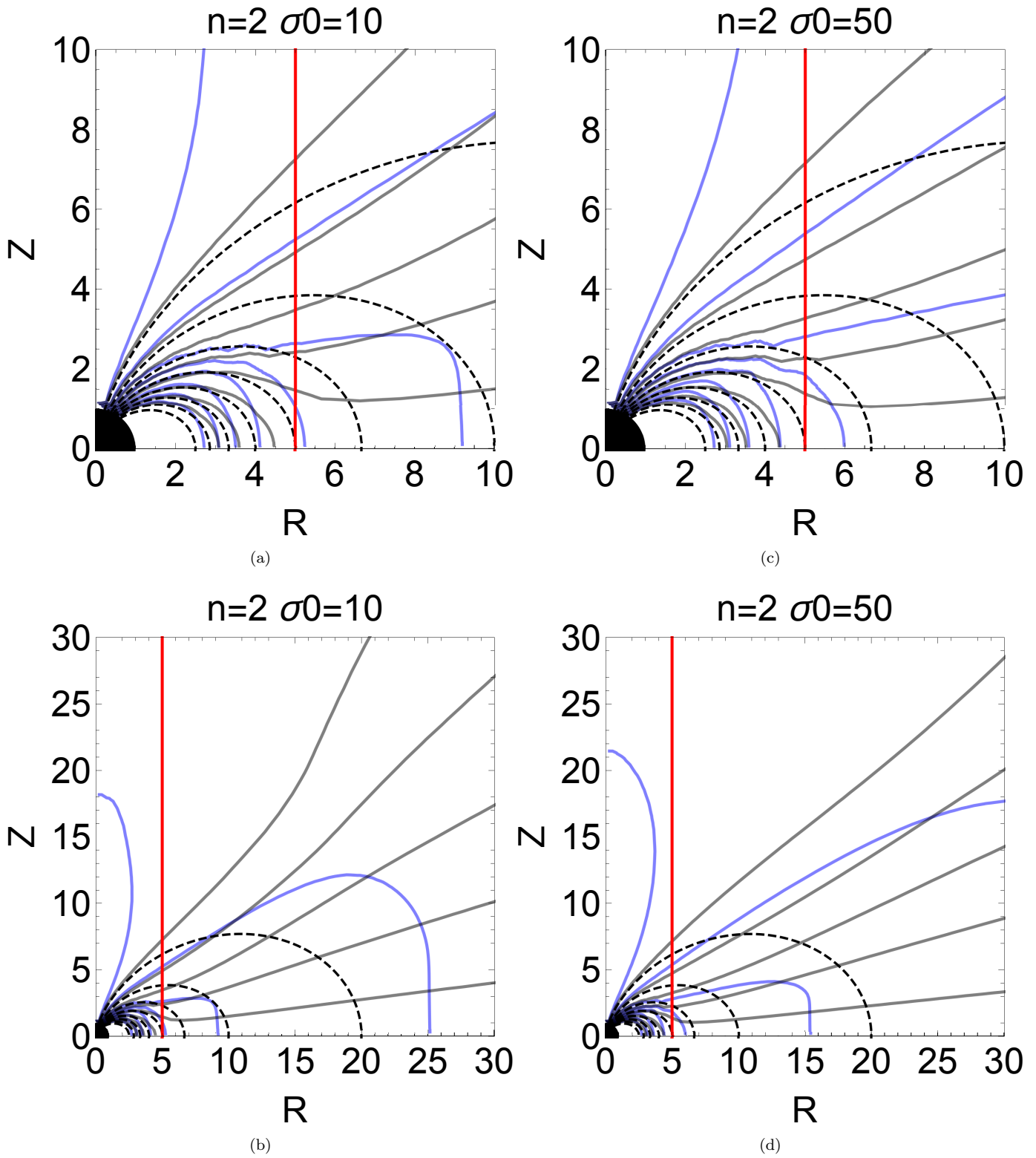


Figure 5. Electrical potential Φ for $n = 2, \sigma_0 = 10, 50$. The red line is the light cylinder radius $R = 5$. The black line is the equal value of the poloidal-magnetic flux function G . The black dotted line shows a dipole magnetic flux equal to the value of the function. Bottom is zoom out view.

nents perpendicular to the magnetic lines of force become dominant.

Figs. 6(e) and (f) are each of the poloidal current densities in the cases where $\sigma_0 = 50$.

4.1.5. Poynting flux

Poynting flux is present because there is a nonzero cross product of the electric and magnetic fields; it Poynting is emitted from the surface outward. I calculated the Poynting flux for the obtained steady solution. Figs. 10 and 11 depict the magnitude and direction distributions of the Poynting vector. The magnitude of the Poynting vector increases from blue to red. As shown in Fig. 3, Poynting flux has a maximum value at the position of the light cylinder, and decreases gradually outside.

The Poynting flux passing through the light cylinder is important. Thus I calculated the Poynting flux's R component, $L_R(R)$, summing up over Z direction:

$$L_R(R) = 2\pi R \int_0^{z_{\max}} (E_\phi B_z - E_z B_\phi) dz. \quad (51)$$

Figure 12 shows that the normalized Poynting flux settles from the inside to the outside over time. Figure 13 plots the distance dependence of normalized pointing flux on the light cylinder.

Poynting flux decreases with radius because the toroidal magnetic field S does not spread to the outside.

In the small conductivity case, Poynting flux decreases rapidly with distance from the surface. Current circuit structure form within a small region. Poynting flux increases linearly with respect to electrical conductivity σ_0 in the light cylinder. However, Poynting flux outside of the light cylinder is not linearly proportional to electrical conductivity σ_0 ; this is because the spatial width of the current circuit is changed by the electrical conductivity. A large spatial scale poloidal current causes a large spatial toroidal magnetic field area. This is evident in the distribution of the toroidal field S under changing electrical conductivity.

4.2. Electrical conductivity (σ_0) dependence of magnetosphere and Poynting flux

Under the same field from the equation of current density model, the current along the magnetic field is increased by high electrical conductivity. However, it is not a solution that is proportional to the electric conductivity due to its non-linearity. The most significant change is dependent upon the electrical conductivity σ_0 , as it adjusts the spatial scale of the current circuit. Circuits are smaller when the electrical conductivity σ_0 is

small. Conversely, the high the electric conductivity σ_0 , the current circuit becomes large. As can be seen from the current density distribution, the spatial structure of the current circuit is difficult to grasp clearly. Therefore, instead of the current density distribution, consider the toroidal magnetic field distribution. Fig.4.1 show contours of the toroidal magnetic field S, which is proportional to the electrical conductivity. Contours have a shape that extends further outward, rather than remaining at the same location. From the results mentioned above, the current circuit expands by increasing the electrical conductivity.

The contour level is five times larger in Fig.6(d) than in Fig.6(a). The maximum toroidal magnetic field S become about five times larger between the $\sigma_0 = 10$ and $\sigma_0 = 50$ cases. Other σ_0 parameters suggest similar results.

In the near-star region and farther out, the toroidal magnetic-field strength is of the same order and shape.

At around $r > 20$, the toroidal magnetic field S gradually decreases outward. Magnetic field lines remain open, but current is insufficient to create a toroidal magnetic field.

In Figs. 6, poloidal current is small in the blue region. Two characteristic structures appear in Figs.6: the equatorial plane and the closed region.

Radial Poynting flux L_R made by B_ϕ and E_z components. This section discusses the Poynting flux dependence of the electric conductivity.

4.2.1. $n = 2$ Case

We set different electric conductivities σ_0 on the star surface, $\sigma_0 = \sigma(r = 1)$. The radial index is set to $n = 2$. Fig. 14 shows the regularized Poynting flux to surface electric conductivity σ_0 . Poynting flux is integrated over the light cylinder radius $R_{LC} = c/\Omega$, and is proportional to electric conductivity σ_0 .

From the fitting result, the linear coefficient is $3.7 \times 10^{-3} L_0/\sigma$, where the normalized Poynting flux is $L_0 = \mu^2 \Omega^4 / c^3$.

4.2.2. $n = 1$ Case

Fig.14 and Fig.15 show the Poynting flux decrease by radius. Poynting flux L depend upon electrical conductivity σ_0 , but the Poynting flux in $n = 1$ is clearly less than in the $n = 2$ case, because the poloidal-current circuit for the $n = 2$ case expands more narrowly than for $n = 1$. The Poynting flux for the $n = 1$ case is not clearly proportional to the electric conductivity.

5. DISCUSSION

5.1. The global magnetospherical structure's electrical-conductivity dependence

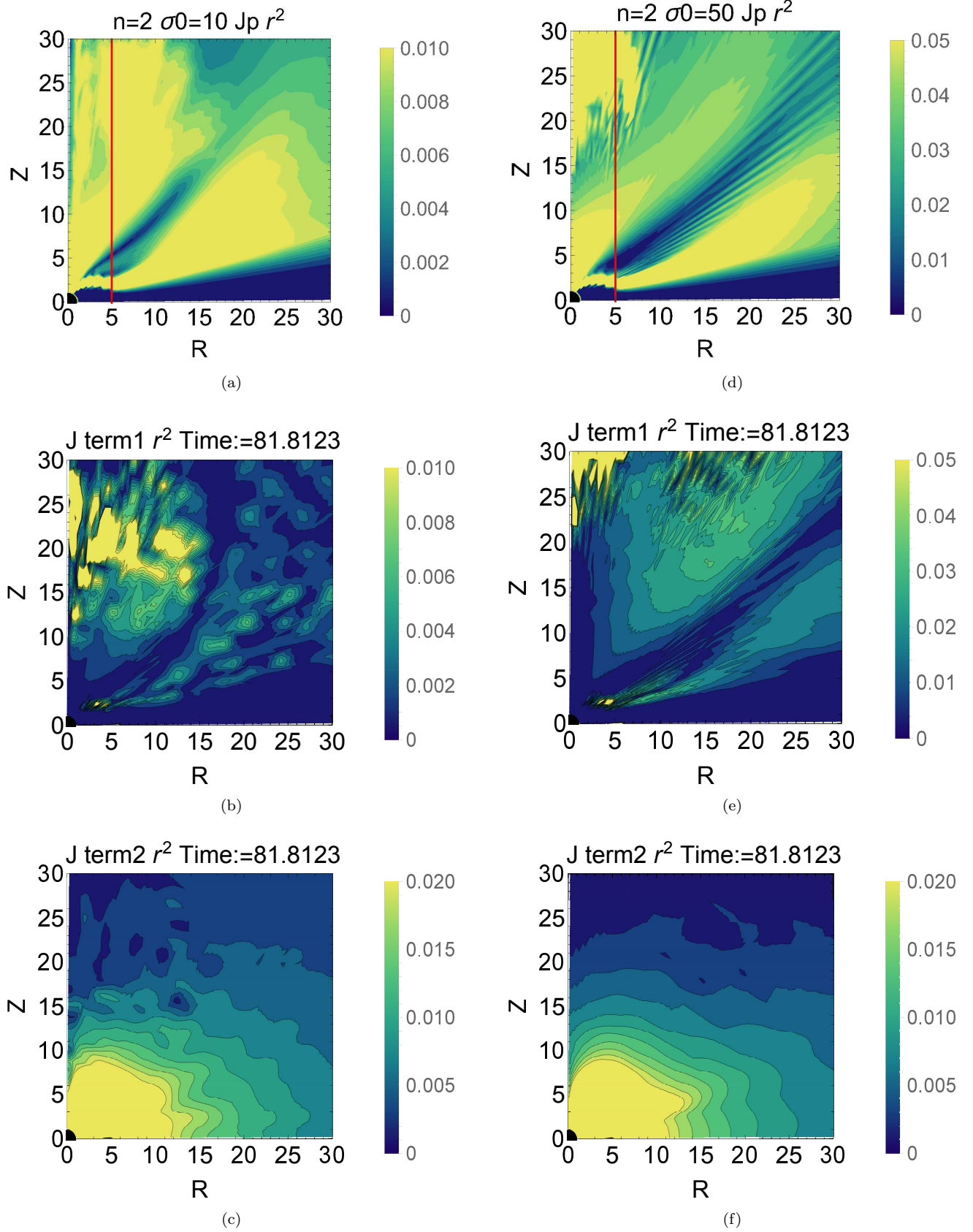


Figure 6. Top:Poloidal current density $j_p r^2$ for $n = 2, \sigma_0 = 10, 50$. Middle:Poloidal current density of first term component in eq.(17) for $\sigma_0 = 10, 50$. Bottom:Poloidal current density of second term component in eq.(17) for $\sigma_0 = 10, 50$.

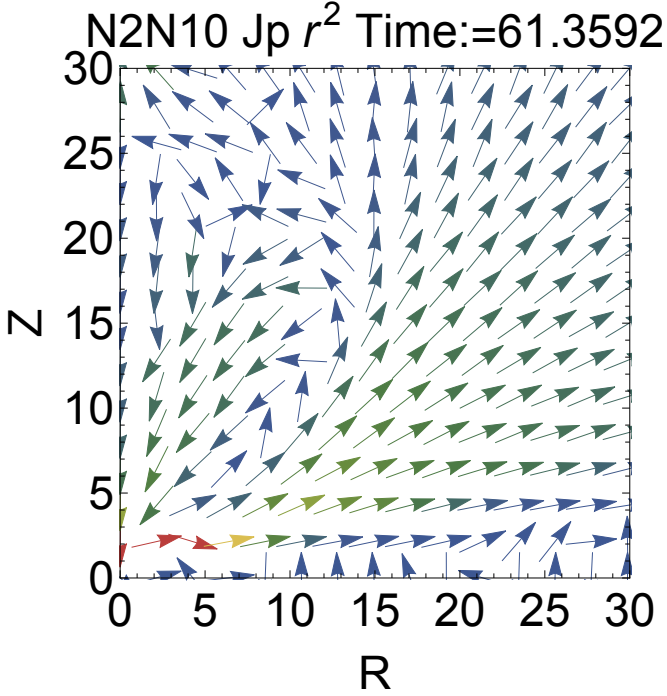


Figure 7. For $n = 2, \sigma_0 = 10$. Poloidal current vector direction shown in the meridional plane. The color of the vector indicates the intensity of poloidal current from blue to red.

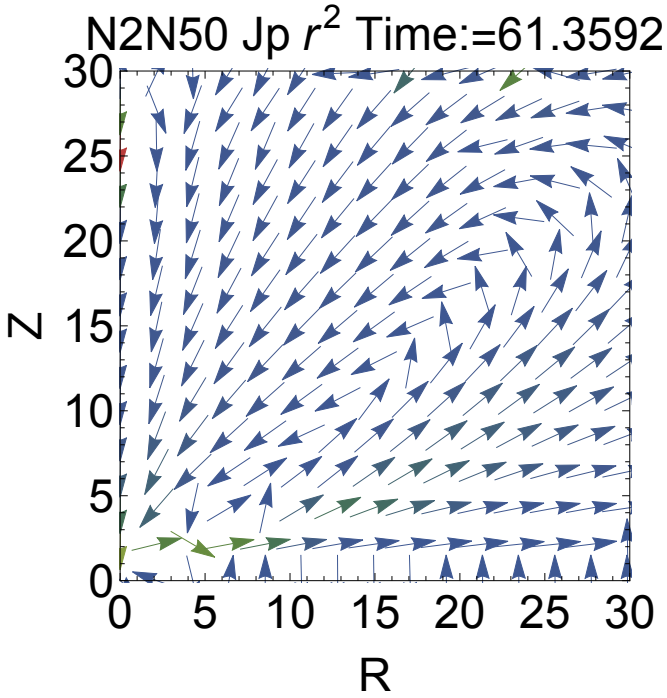


Figure 8. Same as Fig.7 for $\sigma_0 = 50$.

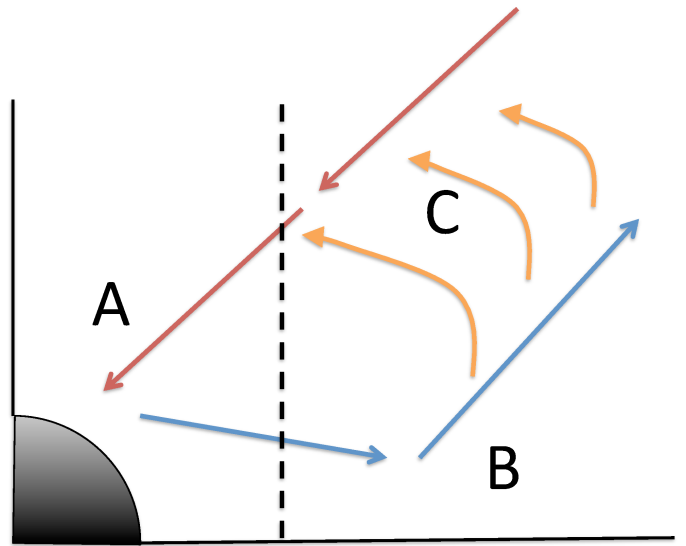


Figure 9. This diagram shows poloidal current circuit. The A and B arrows are the current flow along with the magnetic field. The C arrow shows the current perpendicular to the magnetic-field line. This current circuit shows the toroidal magnetic field.

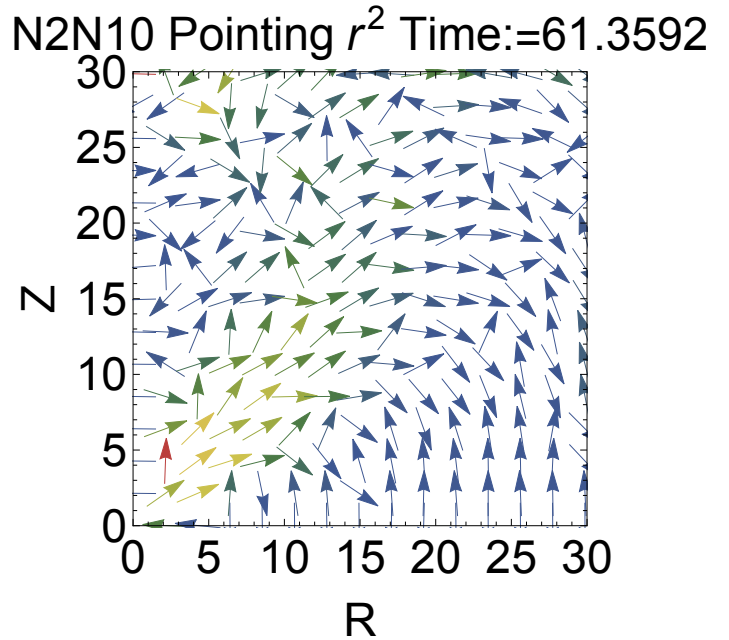


Figure 10. For $n = 2, \sigma_0 = 10$. Vector diagram of Poynting flux. The intensities of the vectors increase in the order blue, green, yellow, red.

Our simulation introduces the radial dependency the of electric conductivity $\sigma(r)$, eq. (49). $\sigma(r)$ is parameterized by n and σ_0 . The current density is derived from Ohm's law; however, the current density includes velocity along the magnetic field as a parameter and cannot be determined uniquely.

N2N50 Pointing r^2 Time:=61.3592

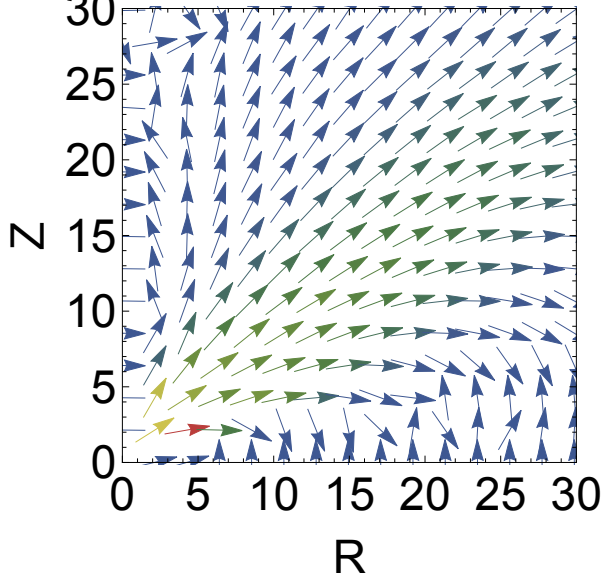


Figure 11. Same as Fig. 10 for $n = 2, \sigma_0 = 50$

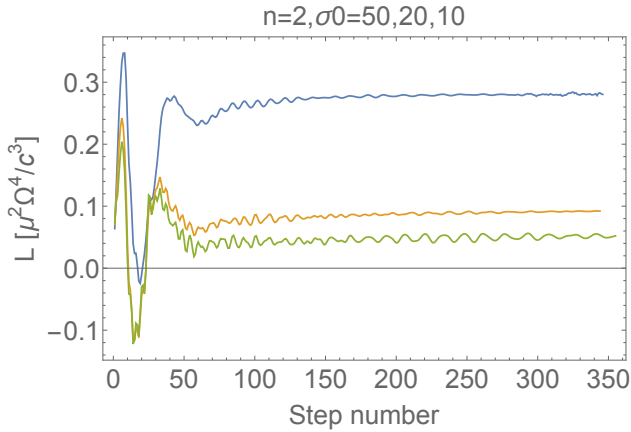


Figure 12. The horizontal axis shows the number of steps, and the vertical axis indicates the normalized Poynting flux. Each line can be seen that converges to a constant value at $\sigma_0 = 10, 20, 50$ for more than time 70 steps, meaning that the magnetosphere is in a stable state over time.

Poynting flux increases monotonically along with electrical conductivity σ_0 because toroidal magnetic field is increased by a large poloidal current. In both the $n=1$ case and $n=2$ cases, Poynting flux is not linearly dependent on the parameters. The poloidal current circuit has width and circuit shape. Poynting flux gradually decreases outward. In the case of $n = 1$, Poynting flux increases gradually compared to the $n = 2$ case. It is found that in the $n = 1$ case, the current circuit is more widely spread than in the $n = 2$ case.

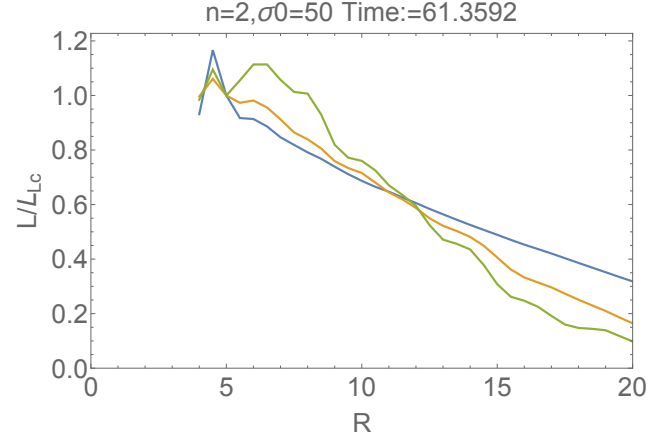


Figure 13. The vertical axis Poynting fluxes are normalized by the value of the light cylinder, while the horizontal axis is the distance from the magnetic axis. Poynting flux is maximal at light cylinder $R = 5$ and is attenuated outside. The green, yellow, and blue lines correspond to $\sigma_0 = 10, 20, 50$. When the electrical conductivity decreases, the Poynting flux damping appear.

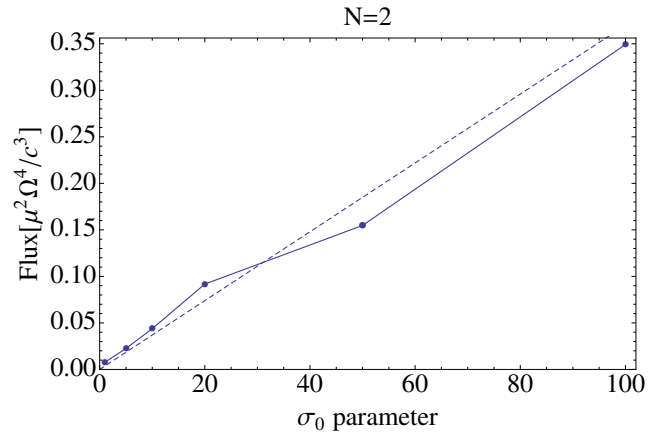


Figure 14. Normalized Poynting flux $L/(\mu^2\Omega^4/c^3)$ across the light cylinder of electric conductivity σ_0 for $n = 2$.

Table 1. Normalized Poynting flux L/L_0 across the light cylinder of electric conductivity σ_0 for $n = 2$.

σ_0	σ_0/Ω	L/L_0
1	5	0.0078
5	25	0.0225
10	50	0.0438
20	100	0.0917
50	250	0.1548
100	500	0.3492
150	750	0.6032

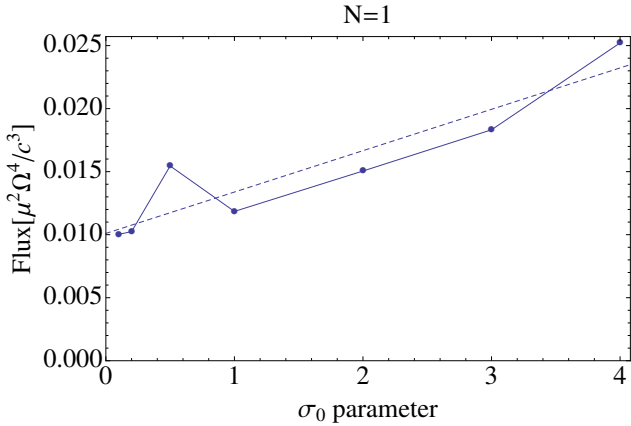


Figure 15. Same as Fig. 14 for $n = 1$.

Table 2. Normalized Poynting flux L/L_0 across the light cylinder of electric conductivity σ_0 for $n = 1$.

σ_0	σ_0/Ω	L/L_0
0.1	0.5	0.0100
0.2	1.0	0.0102
0.5	2.5	0.0155
1	5	0.0118
2	10	0.0151
3	15	0.0183
4	20	0.0252

To compared to other research results in the parameter σ/Ω . In previous papers, only σ_0 has been considered as a parameter. Thus, I use the value of $\sigma(r = 5)/\Omega$. The magnitude of the Poynting flux in each of the parameter is different.

From the force-free simulation result by Spitkovsky (2006), the Poynting flux is

$$\frac{L}{L_0} = (1 + \sin^2 \alpha), \quad (52)$$

where α is the angle between the rotation and magnetization axes. $\alpha = 0$ corresponds to an aligned rotator. Poynting flux is smaller than that in the paper Li et al. (2011).

Li et al. (2011) shows the Poynting flux in the resistive force-free condition. In the $n = 2$ case, we have

$$\frac{L}{L_0} = -2.3 \times 10^{-3} + 1.9 \times 10^{-2} \left(\frac{\sigma}{\Omega} \right). \quad (53)$$

In the $n = 1$ case, we have

$$\frac{L}{L_0} = 1.2 \times 10^{-2} + 8.3 \times 10^{-4} \left(\frac{\sigma}{\Omega} \right). \quad (54)$$

Li et al. (2011) corresponds to the case of $n = 0$. In this case, the electric current is spread more widely than in the $n = 1$ and $n = 2$ cases. Our simulation outer electric conductivity close to vacuum. Thus, Poynting flux becomes small. Poynting flux in the light cylinder is proportional to electrical conductivity. It is different from their result.

5.2. The magnetospheric structure independent of the surface-boundary toroidal magnetic field

Current circuits connect to the star surface; however, the toroidal magnetic field set boundary $B_\phi = 0$ eq.(32). To check whether the toroidal magnetic field of the star surface affects the magnetosphere, a calculation was performed under different surface toroidal magnetic field conditions. The toroidal magnetic field in the surface boundary set $S(r, \theta) = \alpha_s S_0(r, \theta)$, and parameter changed $\alpha_s = 0.5, 1.0, 2.0, 3.0$. The resulting magnetic field is shown in Fig.16. The results show that the Poynting flux does not change for parameter α_s . Poynting flux L is independent of the surface toroidal magnetic field. The magnetic field formed by the current circuit can be considered independent.

5.3. Solve both hemispheres in the magnetosphere

Solutions that dose not form magnetic field line structures may remain open for a closed configuration. This result is in contrast to other studies showing that magnetic field lines gradually opened under strong toroidal current flows in the equatorial plane. In this study, the electrical conductivity in the equatorial plane is set to be the same as in other region. Fig. 17 shows the results, which predict the magnetosphere grows unstable overtime. Color represents the toroidal magnetic field. Instability was developed in the vicinity of the Y-point and equatorial plane beyond the light cylinder. When the electrical conductivity is large, instability grows faster. In the closed magnetic field configuration case, electric conductivity can range up to $\sigma_0 \sim 60$. In the open-boundary-condition case, electrical conductivity can range up to $\sigma_0 = 150$.

5.4. Equatorial plane current sheet

The equatorial plane boundary condition is set as $E_\theta = 0$. The radial magnetic direction is antiparallel to the upper and lower equatorial planes. In center of the current sheet, the magnetic field is very weak. There is no boundary condition for E_r . Thus $E^2 > B^2$ does not meet the force-free condition. The force-free split-monopole and dipole solution has the same character to the current-sheet formation. The split monopole yields a magnetic flux of $f(Z/R)$. From Ampe're's law,

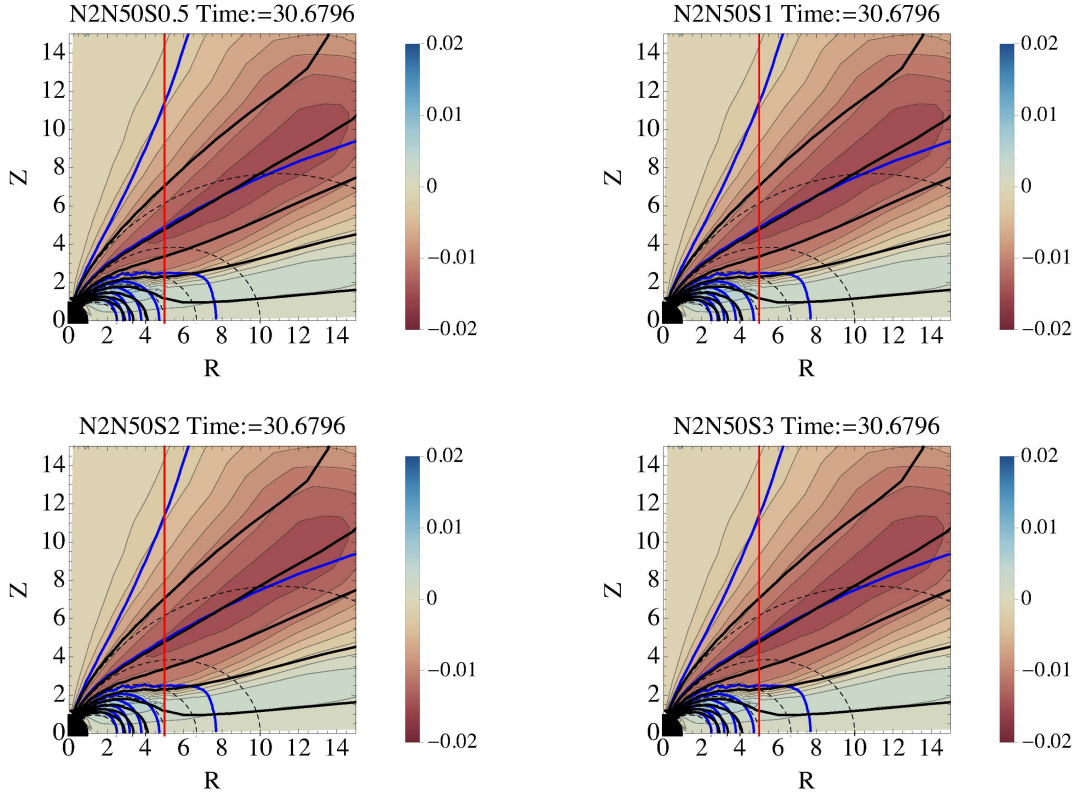


Figure 16. Poloidal and toroidal magnetic field meridional plane by surface change S . Top to bottom and left to light: $S(r, \theta) = \alpha_s S_0(r, \theta)$, parameter $\alpha_s = 0.5, 1.0, 2.0, 3.0$

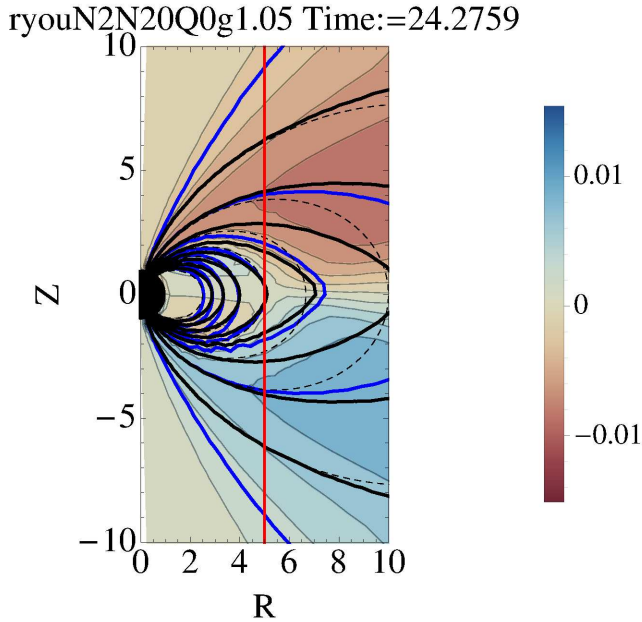


Figure 17. Whole spherical simulation result. Same as Fig.3 for $n = 2, \sigma_0 = 20$

a poloidal magnetic field open in infinite distance needs a toroidal current sheet in the equatorial plane. The equatorial toroidal current sheet is described using the Dirac delta function. In the dipole magnetic field case, electric current concentrates in the last open field line. In this paper, the equatorial plane boundary condition is idealized to solve problems.

6. CONCLUSION

I use a current model derived from Ohm's law to understand resistive force-free magnetospheres. I introduce an electrical conductivity dependent upon distance from the star. A steady state is obtained by combining Maxwell equations and the boundary condition. These resistive force-free solutions show that the current has width and circuit shape. A toroidal magnetic field is formed outside of the light cylinder. The Poynting flux from magnetosphere has a maximum in the light cylinder and decreases on the outside. In the high-conductivity case, the current circuit spreads more widely. The shape of the current circuit varies with the spatial dependence of the electrical conductivity. The Poynting flux in the light cylinder is in proportion to the

electrical conductivity. The surface toroidal magnetic field does not affect Poynting flux in the light cylinder.

ACKNOWLEDGMENT

The author is thankful to Yasufumi Kojima for many useful comments and their help with the code.

REFERENCES

- Cerutti, B., Philippov, A., Parfrey, K., & Spitkovsky, A. 2015, *\mnras*, 448, 606
- Cerutti, B., Philippov, A. A., & Spitkovsky, A. 2016, *Monthly Notices of the Royal Astronomical Society*, 457, 2401
- Chen, A. Y., & Beloborodov, A. M. 2014, 13
- Contopoulos, I., Kazanas, D., & Fendt, C. 1999, *The Axisymmetric Pulsar Magnetosphere*
- Goldreich, P., & Julian, W. H. 1969, *The Astrophysical Journal*, 157, 869
- Gruzinov, A. 2005, *Physical Review Letters*, 94, 1
- . 2007, 2, 4
- . 2008, *Arxiv preprint*, 6
- . 2011, *New York*, 3
- Kalopotharakos, C., Kazanas, D., Harding, A., & Contopoulos, I. 2012, *The Astrophysical Journal*, 749, 2
- Komissarov, S. S. 2006, *Monthly Notices of the Royal Astronomical Society*, 367, 19
- Krause-Polstorff, J., & Michel, F. C. 1985, *Monthly Notices of the Royal Astronomical Society (ISSN 0035-8711)*, vol. 213, March 15, 1985, p. 43P-49P.
- Li, J., Spitkovsky, A., & Tchekhovskoy, A. 2011, *Arxiv preprint*, 13
- Lyutikov, M. 2003, *Monthly Notices of the Royal Astronomical Society*, 346, 540
- McKinney, J. 2006, *\mnras*, 368, L30
- Pétri, J. 2009, *Astronomy and Astrophysics*, 503, 1
- Philippov, A., & Spitkovsky, A. 2014, *\apjl*, 785, L33
- Philippov, A., Spitkovsky, A., & Cerutti, B. 2015, *\apjl*, 801, L19
- Spitkovsky, A. 2006, 1
- Tchekhovskoy, A., Spitkovsky, A., & Li, J. G. 2013, *Monthly Notices of the Royal Astronomical Society: Letters*, 435, L1
- Timokhin, A. 2006, *Monthly Notices of the Royal Astronomical Society*, 368, 1055